Small-Signal Modeling and Networked Control of a PHEV Charging Facility

Luis Herrera, *Student Member, IEEE*, Ernesto Inoa, *Member, IEEE*, Feng Guo, *Student Member, IEEE*, Jin Wang, *Member, IEEE*, and Hanning Tang, *Member, IEEE*

***Abstract*—The introduction of communication systems to power system controllers has brought in another layer of complexity in their design and operation. In this paper, a plug-in hybrid electric vehicle charging facility is studied. A linearized model of the facility is built, including both the dc/dc and dc/ac converters of the distributed energy resources. In addition, a control strategy that includes both local and networked loops is proposed to monitor and control the dc bus voltage of a local energy storage unit. This dc bus voltage is crucial to the self-sustaining capabilities of the system. A review of challenges and opportunities in networked control systems is presented, and the impacts of communication factors to the charging facility stability are analyzed. Finally, a real-time simulation platform which combines both electrical and communication networks is presented to validate the small-signal model, control strategy, and stability analysis including the communication effects.**

***Index Terms*—AC–DC power converters, dc–dc power converters, networked control systems (NCSs), power system stability, smart grid.**

I. Introduction

With the need to supply clean renewable energies, integrations of distributed energy resources (DERs) into plug-in hybrid electric vehicle (PHEV) charging facilities are expected. One key aspect of this integration is the introduction of communication systems to multiple power units in the facility, including both sources and loads. The addition of communication networks presents both opportunities and challenges in the control and optimization strategies to provide highest efficiency and ancillary services such as frequency and voltage regulation, VAR compensation, etc. [1].

In a typical charging facility, charging stations need to be equipped with local controllers and communication systems. For example, it is necessary for the charging facility to know the state of the grid in terms of demand, pricing, and health status in order to better estimate optimal charging schedules. In [2], overviews of different communication methods applicable to PHEV charging stations such as power line carriers, IEEE 802.15.4 (ZigBee), ZWave, and cellular networks were summarized and compared. While in [3], a ZigBee-based platform for testing optimization parameters in a PHEV charging station was proposed and studied.

The reliability of the charging facility can be considered to depend on two modes of operation: grid connected and islanded. Several papers have addressed optimal strategies and the stability of microgrids by studying the small-signal model of the system. In these papers, inverter-based models of microgrids have been constructed by assuming that the dc and/or ac voltage sources are ideal [4], [5]. For instance, in [5], a systematic approach for small-signal stability analysis of an inverter-based microgrid with simplified dc input was proposed and verified. However, to boost voltage and to increase system-level efficiency, a boost converter is often added between the dc source and the dc/ac inverter. In addition, depending on the control strategy of the dc/dc and dc/ac converters, the simplification of the dc side cannot be applied to all cases. For this reason, in this paper, we present a method to model both the dc/dc and dc/ac converters of a DER which has not been discussed in previous literatures.

Furthermore, the introduction of communication as an integral part of a controller is known as a networked control system (NCS) [6]. In this case, a stability analysis needs to be performed under different communication factors such as delay, packet losses, etc. In [7], the authors have studied the operation of parallel dc/dc converters using wireless signals to transmit sensor data. In [8], an NCS for wide-area power systems was designed and simulated. Finally, in [9], the authors presented a case for distributed and central droop control through communication links. However, in the latter, the stability of the microgrid was studied only through simulations.

In this paper, an instance of networked control of a PHEV charging facility is developed and analyzed. In Section II, the small-signal model of the charging facility, including multiple DERs with two-stage (dc/dc cascaded by dc/ac) power converters, is built. Utilizing this linearized model, an approach of applying NCS to the charging facility is proposed in Section III. In addition, a summary of the challenges when studying NCS is presented. The model and stability analysis are then verified using real-time simulations. The real-time platform is presented in Section IV, and the stability analysis results are presented in

Manuscript received November 28, 2012; revised March 24, 2013; accepted June 2, 2013. Date of publication July 11, 2013; date of current version March 17, 2014. Paper 2012-IPCC-635.R1, presented at the 2012 IEEE Energy Conversion Congress and Exposition, Raleigh, NC, USA, September 15–20, and approved for publication in the IEEE Transactions on Industry Applications by the Industrial Power Converter Committee of the IEEE Industry Applications Society.

L. Herrera, F. Guo, and J. Wang are with the Department of Electrical and Computer Engineering, The Ohio State University, Columbus, OH 43210 USA (e-mail: herrera.46@buckeyemail.osu.edu; guof@ece.osu.edu; wang@ece.osu.edu).

E. Inoa is with Caterpillar, Inc., Peoria, IL 61629 USA (e-mail: einoa@ieee.org).

H. Tang is with Eaton Corporation, Arden, NC 28704 USA (e-mail: hanningtang@eaton.com).

Color versions of one or more of the figures in this paper are available online at http://ieeexplore.ieee.org.

Digital Object Identifier 10.1109/TIA.2013.2272912

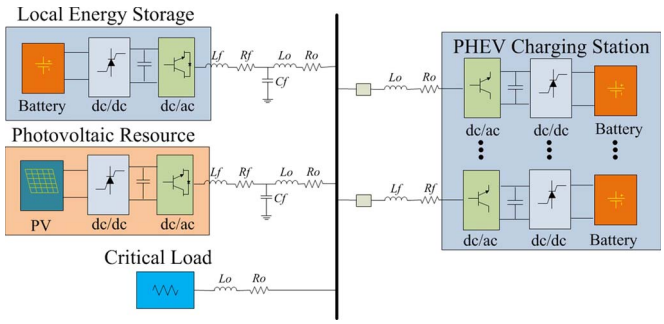

Fig. 1. Topology of the charging facility.

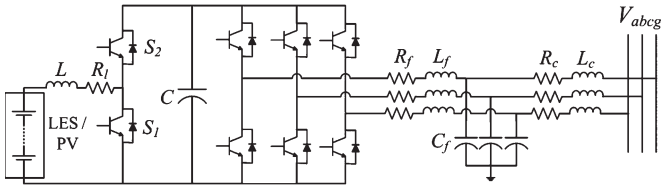

Fig. 2. Power converter structure in the LES and PV resources.

Section V. The conclusion and a summary of future work are then stated in Section VI.

II. Modeling of the Charging Facility

Nowadays, PHEV charging facilities with renewable-energy sources are becoming an important topic of study due to the capabilities of mitigating the impact of PHEV loads to the grid. For example in [10], a control strategy for power balancing for a PHEV charging facility with photovoltaic (PV) was presented. Furthermore, in [11], a local energy storage (LES) unit is proposed along with a dc network, and in [12], a design optimization for a charging installation with wind and PV DERs was analyzed.

A PHEV charging facility can be considered as a small microgrid when coupled with DERs. Typical strategies such as droop control for balancing DER power could be applied to an installation. The PHEV charging facility discussed in this paper has two integrated DER units: a LES and a PV plant aimed for level 2 charging power [13]. The structure of this facility is shown in Fig. 1. The modeling and analysis of a self-sustainable islanded facility is studied. In order to derive a mathematical model for the system, the power converters, the controllers, and the loads are taken into account.

A. Power Converters

The LES and PV DER power converter structure is shown in Fig. 2. This model is split into two parts: the dc/dc boost and the dc/ac inverter.

1) DC/DC Converter: State space averaging is used in order to model the open-loop boost converter [14]. The average differential equations are given by

$$\dot{x} = (dA_{\text{on}} + (1-d)A_{\text{off}})\,x + (dB_{\text{on}} + (1-d)B_{\text{off}})\,u$$
$$\dot{x} = f(x,u) \tag{1}$$

where $u = [d, V_{\text{dc}}, i_o]^{\text{T}}$ contains the duty cycle, dc input voltage (LES or PV), and output current (input from dc/ac side). The system is then linearized around an equilibrium point $m^* := (X^*, U^*)$ by defining a new set of variables $\tilde{x} := x - x^*$, $\tilde{u} := u - u^*$. The state variables are the inductor current and the capacitor voltage $\tilde{x} = [\tilde{i}_L, \tilde{v}_C]^{\text{T}}$. The linearized equations for the boost converter are then

$$\frac{d}{dt}\begin{pmatrix}\tilde{i}_L\\ \tilde{v}_C\end{pmatrix} = \begin{pmatrix}\frac{-R_l - R_m D^*}{L} & \frac{-(1-D^*)}{L}\\ \frac{(1-D^*)}{C} & 0\end{pmatrix}\begin{pmatrix}\tilde{i}_L\\ \tilde{v}_C\end{pmatrix} + \begin{pmatrix}\frac{1}{L}\\ 0\end{pmatrix}\tilde{V}_{\text{dc}} + \begin{pmatrix}\frac{V_c^* - I_L^* R_m}{L}\\ -\frac{I_L^*}{C}\end{pmatrix}\tilde{d} + \begin{pmatrix}0\\ -\frac{1}{C}\end{pmatrix}\tilde{i}_o. \tag{2}$$

2) DC/AC Inverter: The modeling of the dc/ac inverter involves the analysis of the *LCR* low-pass filter, the coupling inductance, and the line resistance. Prior to deriving the differential equations for the open-loop inverter, the power invariant abc to dq transformation is used to simplify the analysis. After applying this transformation, the system is linearized around an equilibrium point given by $\eta^* := (X^*, D^*, V_C^*, V_g^*)$. The linearized equations are the following:

$$\frac{d}{dt}\begin{pmatrix}\tilde{i}_d\\ \tilde{i}_q\\ \tilde{v}_{fd}\\ \tilde{v}_{fq}\\ \tilde{i}_{cd}\\ \tilde{i}_{cq}\end{pmatrix} = \begin{pmatrix}\frac{-R_f}{L_f} & \omega_n & \frac{-1}{L_f} & 0 & 0 & 0\\ -\omega_n & \frac{-R_f}{L_f} & 0 & \frac{-1}{L_f} & 0 & 0\\ \frac{1}{C_f} & 0 & 0 & \omega_n & \frac{-1}{C_f} & 0\\ 0 & \frac{1}{C_f} & -\omega_n & 0 & 0 & \frac{-1}{C_f}\\ 0 & 0 & \frac{1}{L_c} & 0 & \frac{-R_c}{L_c} & \omega_n\\ 0 & 0 & 0 & \frac{1}{L_c} & -\omega_n & \frac{-R_c}{L_c}\end{pmatrix} \times \begin{pmatrix}\tilde{i}_d\\ \tilde{i}_q\\ \tilde{v}_{fd}\\ \tilde{v}_{fq}\\ \tilde{i}_{cd}\\ \tilde{i}_{cq}\end{pmatrix} + \begin{pmatrix}\frac{V_c^*}{L_f} & 0\\ 0 & \frac{V_c^*}{L_f}\\ 0 & 0\\ 0 & 0\\ 0 & 0\\ 0 & 0\end{pmatrix}\begin{pmatrix}\tilde{d}_d\\ \tilde{d}_q\end{pmatrix} + \begin{pmatrix}\frac{D_d^*}{L_f} & 0 & 0\\ \frac{D_q^*}{L_f} & 0 & 0\\ 0 & 0 & 0\\ 0 & 0 & 0\\ 0 & \frac{-1}{L_c} & 0\\ 0 & 0 & \frac{-1}{L_c}\end{pmatrix}\begin{pmatrix}\tilde{v}_c\\ \tilde{v}_{gd}\\ \tilde{v}_{gq}\end{pmatrix}. \tag{3}$$

In order to link the small-signal models of the dc/dc converter and dc/ac inverter together, the relationship between the voltages and currents of the two circuit stages can be written as [15]

$$v_{id} = v_C d_d \tag{4}$$
$$v_{iq} = v_C d_q \tag{5}$$
$$i_o = i_d d_d + i_q d_q. \tag{6}$$

Although (4) and (5) were already taken into account in (3), (6) can be connected to the dc/dc converters by linearizing

$$\tilde{i}_o = I_d^* \tilde{d}_d + I_q^* \tilde{d}_q + \tilde{i}_d D_d^* + \tilde{i}_q D_q^* \tag{7}$$

and linking (7) to (2).

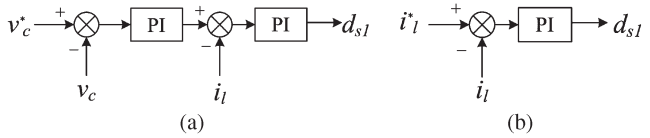

Fig. 3. DC/DC closed-loop controllers for LES and PV, respectively. (a) LES dc/dc controller. (b) PV dc/dc controller.

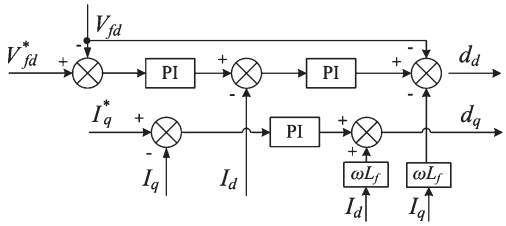

Fig. 4. LES dc/ac controller.

B. LES and PV DER Controllers

The control structure of the LES and PV power converters is quite different. More specifically, the LES regulates the main ac bus voltage, while the PV injects maximum active power to the charging facility.

1) LES Controller: The dc/dc controllers of the LES and PV converters are shown in Fig. 3. In order to write the linearized closed-loop system of the LES boost converter, the proportional and integral (PI) controllers can be represented by adding two state variables to the system

$$\begin{aligned}\dot{\xi}_{\mathrm{Ldc1}} &= -\tilde{v}_C \\ \dot{\xi}_{\mathrm{Ldc2}} &= -kp_{\mathrm{Ldc}v}\tilde{v}_C + ki_{\mathrm{Ldc}v}\xi_1 - \tilde{i}_L. \end{aligned} \tag{8}$$

Thus, the closed-loop state variables are $\tilde{x}_{cl} = [\tilde{i}_L, \tilde{v}_c, \xi_{\mathrm{Ldc1}}, \xi_{\mathrm{Ldc2}}]^{\mathrm{T}}$, and the input duty cycle is then

$$\tilde{d} = (-kp_{\mathrm{Ldc}v}\tilde{v}_C + ki_{\mathrm{Ldc}v}\xi_{\mathrm{Ldc1}} - \tilde{i}_L)kp_{\mathrm{Ldc}i} + \xi_{\mathrm{Ldc2}}ki_{\mathrm{Ldc}i}. \tag{9}$$

This controller regulates the dc link voltage to maintain it at a fixed value.

The dc/ac controller of the LES is shown in Fig. 4. In order to model the closed-loop converter for the LES, three additional state variables are introduced in the same manner as for the dc/dc controller $[\xi_{\mathrm{Lac1}}\ \xi_{\mathrm{Lac2}}\ \xi_{\mathrm{Lac3}}]^{\mathrm{T}}$; based on these new variables, the modulation factors in both the d- and q- axes can be derived as

$$\begin{aligned}\tilde{d}_d &= (-\tilde{v}_{fd}kp_{\mathrm{Lac}v} + \xi_{\mathrm{Lac1}}ki_{\mathrm{Lac}v} - \tilde{i}_d) \\ &\quad \times kp_{\mathrm{Laci}} + \xi_{\mathrm{Lac2}}ki_{\mathrm{Laci}} - \tilde{v}_{fd} - \tilde{i}_q\omega_n L_f \\ \tilde{d}_q &= -\tilde{i}_q kp_{\mathrm{Lacq}} + \xi_{\mathrm{Lac3}}ki_{\mathrm{Lacq}} + \tilde{i}_d\omega_n L_f. \end{aligned} \tag{10}$$

The closed-loop state space representation for the LES inverter can be obtained by linking the control states and (10) to (3).

2) PV Controller: The PV boost controller is shown Fig. 3(b). This controller regulates the output current of the PV in order to operate at MPPT point. Since the system is linearized about an operating point, it is assumed that this operating point is already at MPPT, and the dynamics of the MPPT algorithm

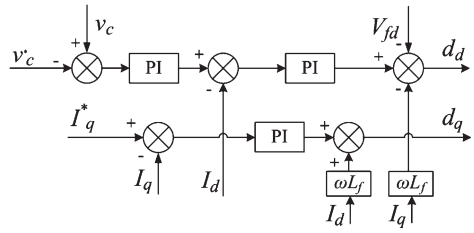

Fig. 5. PV dc/ac controller.

are not considered. This is essentially true for look-up table algorithms.

The controller is modeled in a similar way as that for the LES case. The closed-loop state variables for the PV converter are then $\tilde{x} = [\tilde{i}_L, \tilde{v}_C, \xi_{\mathrm{Pdc1}}]^{\mathrm{T}}$, and the duty cycle becomes

$$\tilde{d}_i = -\tilde{i}_L kp_{\mathrm{Pdc}} + \xi_{\mathrm{Pdc1}}ki_{\mathrm{Pdc}}. \tag{11}$$

Since the boost converter is operating as a current source, the inverter is controlled to maintain a constant dc bus voltage. Therefore, the dc/dc side of the PV plays a very important role and should not be ignored. The controller shown in Fig. 5 can be modeled similarly by introducing three states $[\xi_{\mathrm{Pac1}}\ \xi_{\mathrm{Pac2}}\ \xi_{\mathrm{Pac3}}]^{\mathrm{T}}$, and the modulation factors are

$$\begin{aligned}\tilde{d}_d &= (\tilde{v}_C kp_{\mathrm{Pac}v} + \xi_{\mathrm{Pac1}}ki_{\mathrm{Pac}v} - \tilde{i}_d) \\ &\quad \times kp_{\mathrm{Paci}} + \xi_{\mathrm{Pac2}}ki_{\mathrm{Paci}} - \tilde{v}_{fd} - \tilde{i}_q\omega_n L_f \\ \tilde{d}_q &= -\tilde{i}_q kp_{\mathrm{Pacq}} + \xi_{\mathrm{Pac3}}ki_{\mathrm{Pacq}} + \tilde{i}_d\omega_n L_f. \end{aligned} \tag{12}$$

The closed-loop system for the PV inverter is built in a similar way as that for the LES inverter.

C. Loads and Large-Scale System Model

The PHEV batteries along with their chargers are modeled as a resistor in series with an inductor so as to provide ability to draw both active and reactive power. The equations in the dq-axis for an RL load are

$$\begin{aligned}\frac{di_{d\mathrm{Bat}}}{dt} &= \frac{-R_{\mathrm{Bat}}}{L_{\mathrm{Bat}}}i_{d\mathrm{Bat}} + \omega_n i_{q\mathrm{Bat}} + \frac{1}{L_{\mathrm{Bat}}}d_d v_{gd} \\ \frac{di_{q\mathrm{Bat}}}{dt} &= -\omega_n i_{d\mathrm{Bat}} - \frac{R_{\mathrm{Bat}}}{L_{\mathrm{Bat}}}i_{q\mathrm{Bat}} + \frac{1}{L_{\mathrm{Bat}}}d_q v_{gq} \end{aligned} \tag{13}$$

where R_{Bat} and L_{Bat} stand for the load resistance and inductance, respectively.

In order to have a well-defined main ac bus voltage value $v_g = [v_{gd}\ v_{gq}]^{\mathrm{T}}$ shown in Fig. 2, [5] explains the addition of a virtual resistance r_N in both the d- and q-axes. In the case of the charging facility shown in Fig. 1, this resistance can be made to correspond to the critical loads. The interconnection voltage is then written as

$$\begin{aligned}\tilde{v}_{gd} &= r_N\left(\tilde{i}_d^L + \tilde{i}_d^P - \tilde{i}_{\mathrm{Bat}_d}\right) \\ \tilde{v}_{gq} &= r_N\left(\tilde{i}_q^L + \tilde{i}_q^P - \tilde{i}_{\mathrm{Bat}_q}\right) \end{aligned} \tag{14}$$

where L stands for LES and P stands for PV.

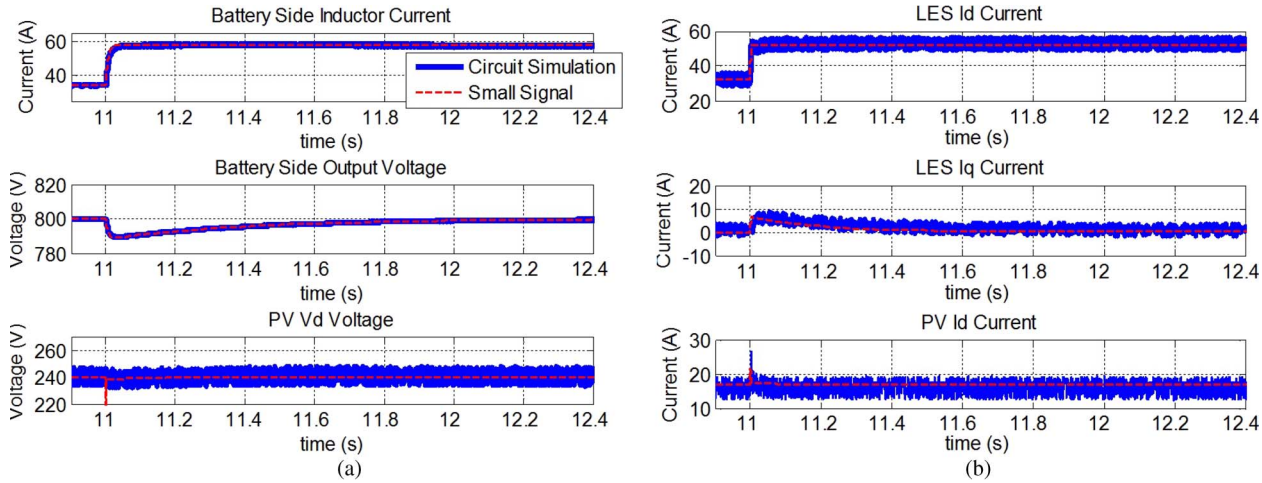

Fig. 6. Small-signal model validation based on circuit simulation. A PHEV battery is connected to the system at $t = 11$ s.

TABLE I
SIMULATION PARAMETERS

PV $V_{dc\text{MPPT}}$	437 V	PV $i_{L\text{MPPT}}$	7.6 A
LES, PV v_C	800 V	Ac Bus V_{gd}	240 V_{rms}
LES V_{dc}	212 V	Critical Load r_N	1000 Ω
Load Dist. $\hat{I}_d$	16.67 A	Fund. Frequency	60 Hz

Once all the subsystems are defined, the complete large-scale state space system can be derived in order to study the stability of the charging facility about an operating point. In addition, this large-scale system will be the basis for the networked control studied in Section III. The linearized model of the charging facility is derived as follows:

$$\begin{pmatrix} \dot{\tilde{x}}_{\text{Ldc}} \\ \dot{\tilde{x}}_{\text{Lac}} \\ \hline \dot{\tilde{x}}_{\text{Pdc}} \\ \dot{\tilde{x}}_{\text{Pac}} \\ \hline \dot{\tilde{x}}_{\text{Bat}} \end{pmatrix} = \left(\begin{array}{cc|cc|c} A^{\text{LES}}_{\text{dc}} & B^{\text{LES}}_{i_o} & 0 & 0 & 0 \\ B^{\text{LES}}_{v_C} & A^{\text{LES}}_{\text{dc/ac}} & 0 & B^{P\to L}_{i_{dq}} & B^{B\to L}_{i_{dq}} \\ \hline 0 & 0 & A^{\text{PV}}_{\text{dc}} & B^{\text{PV}}_{i_o} & 0 \\ 0 & B^{L\to P}_{i_{dq}} & B^{\text{PV}}_{v_C} & A^{\text{PV}}_{\text{dc/ac}} & B^{B\to P}_{i_{dq}} \\ \hline 0 & B^{L\to B}_{i_{dq}} & 0 & B^{P\to B}_{i_{dq}} & A_{\text{Bat}} \end{array}\right) \times \begin{pmatrix} \tilde{x}_{\text{Ldc}} \\ \tilde{x}_{\text{Lac}} \\ \hline \tilde{x}_{\text{Pdc}} \\ \tilde{x}_{\text{Pac}} \\ \hline \tilde{x}_{\text{Bat}} \end{pmatrix} + \begin{pmatrix} \tilde{B}^{L}_{V_{\text{dc}}} & 0 & 0 \\ 0 & 0 & B_{\hat{i}_L} \\ 0 & B^{P}_{V_{\text{dc}}} & 0 \\ 0 & 0 & B_{\hat{i}_P} \\ 0 & 0 & B_{\hat{i}_B} \end{pmatrix} \begin{pmatrix} \tilde{V}^{\text{LES}}_{\text{dc}} \\ \tilde{V}^{\text{PV}}_{\text{dc}} \\ \hat{I}_{dq} \end{pmatrix} \quad (15)$$

where $\hat{I}_{dq}$ is an intentional disturbance added to the system at the load side used to represent PHEV battery connections and to validate the small-signal model. In addition, the off-diagonal elements in the state matrix represent the interconnections given by (4)–(7) and (14). Fig. 6 shows the verification of the linearized model by comparing the analysis results with a circuit simulation of the charging facility in MATLAB/Simulink. The main parameters of the simulation are shown in Table I.

From Fig. 6, it is important to see that, after a PHEV battery is added to the facility, the LES storage supplies its demanded power, while the PV DER output power remains constant since it is assumed to be already supplying maximum active power.

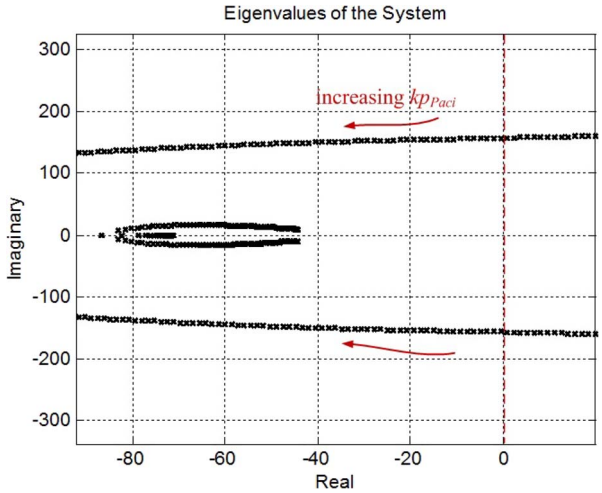

Fig. 7. Eigenvalue placement when varying kp_i of PV ac controller.

D. Eigenvalue Analysis

Once the charging facility model is derived, the eigenvalues of (15) can be studied in order to determine the local stability property of the charging facility and its sensitivity to control parameters. The system in (15) is said to be *locally exponentially stable* if the set of all eigenvalues of the closed-loop state matrix $\sigma(A_{cl}) \subset \mathbb{C}^-$. It is found that the charging facility is particularly sensitive to the PV control parameters as shown in Fig. 7.

It can be clearly seen from Fig. 7 that the control constants should be carefully chosen in order to obtain a safe operation of the charging facility based on the proposed control structure.

The red arrows in Fig. 7 indicate an increase in the value of kp_i.

III. NETWORKED CONTROL OF THE CHARGING FACILITY

For the charging facility presented in Section II, there are several reasons for the involvement of communication networks to enhance the operation and reliability of the facility.

1) Control the power output based on the status of the batteries (SoC, T, etc.).

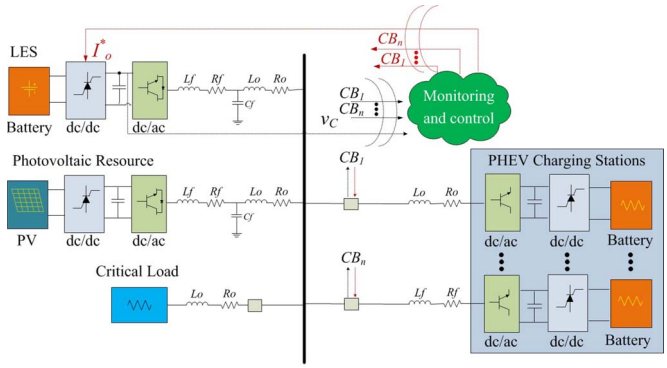

Fig. 8. Charging facility including communication infrastructure.

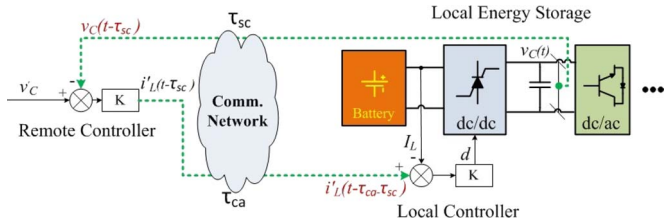

Fig. 9. Proposed controller to monitor and control v_C.

2) During grid-connected mode, decide the best charging times based on a price signal from the grid.
3) Monitor the power output of the LES system for power balancing between the DERs and PHEVs.

Therefore, networked control can be used to determine how communication parameters such as latency and packet losses impact the operation of the charging facility.

A. Proposed Controller

In this paper, a control strategy for power balance is proposed based on monitoring the output voltage of the LES boost converter v_C. This dc bus voltage is an indication of the power-handling capacity of the charging facility. It is assumed that the PV is supplying maximum power at any given time; therefore, the rest of the active loads will be supplied by the LES. If v_C cannot be maintained to a desired value, there is more active power demanded than supplied by the LES and PV. This voltage can be used in deciding whether vehicles should be connected or disconnected or in reducing their charging power. The system diagram with communication is shown in Fig. 8.

In this charging facility, the networked controllers are envisioned to be composed of local and remote control units. Fig. 9 shows a diagram of the proposed controller where the inner loop controls the current and the outer loop incorporates a communication link to monitor and control the v_C voltage. In addition, τ_{sc} and τ_{ca} represent the sensor-to-controller and controller-to-actuator delays, respectively.

B. NCS Modeling

In NCS, there is a need for efficient methods that guarantee the stability of the system under different network parameters such as time-varying transmission times, packet dropouts, and delays. In this section, we review major results achieved in recent years.

1) Transmission Times: Transmission times is the interval between two consecutive transmission measured at the time at which the transmissions arrive [18]. It is analogous to sampling periods if the delays are ignored. In many cases, fixed transmission times denoted by h cannot be guaranteed. For this reason, [17] introduced a sufficient condition for the maximum allowable transmission interval (MATI) for which stability of the closed-loop networked system, as in Fig. 9, is maintained. Let the closed-loop system be represented by

$$\dot{x}(t) = (A - BK)x(t) = A_{\rm cl}x(t) \tag{16}$$

and assume that $\sigma(A_{\rm cl}) \subset \mathbb{C}^-$; then, there exists a positive definite matrix P satisfying the Lyapunov equation $A_{\rm cl}^{\rm T}P + PA_{\rm cl} = -I$. Based on P and defining $\lambda_1 := \lambda_{\min}(P)$ and $\lambda_2 := \lambda_{\max}(P)$, then the MATI satisfies

$$h < \min\left\{\frac{\ln(2)}{p\|A_{\rm cl}\|}, \frac{1}{8\|A_{\rm cl}\|(\sqrt{\lambda_2/\lambda_1}+1)\sum_{i=1}^{p} i}, \frac{1}{16\lambda_2\sqrt{\lambda_2/\lambda_1}\|A_{\rm cl}\|^2(\lambda_2/\lambda_1+1)\sum_{i=1}^{p} i}\right\} \tag{17}$$

where p is the total number of nodes (see [17] for the proof). Moreover, [18] further generalized the MATI constraint for positive definite matrixes P and Q satisfying $A_{\rm cl}^{\rm T}P + PA_{\rm cl} = -Q$, and the MATI constraint is then

$$h < \frac{\lambda_{\min}(Q)}{16\lambda_2\sqrt{\lambda_2/\lambda_1}\|A_{\rm cl}\|^2(\lambda_2/\lambda_1+1)\sum_{i=1}^{p} i}. \tag{18}$$

In this case, the maximum transmission interval is a function of two variables $h = f(P, Q)$, and it is desirable to maximize h. Again, this constraint provides a sufficient condition which may be too conservative. Further results following the same idea as shown previously are presented in [19] and [20].

2) Packet Dropouts: Another impact of NCS is packet losses. These are usually specified by a probability rate r based on the type of network and protocol. In [18], an asynchronous dynamical system (ADS) method for dealing with packet dropouts on the sensor to controller link is presented. Define the following matrixes:

$$\phi_1 = \begin{pmatrix} e^{Ah} & -\Lambda \\ e^{Ah} & -\Lambda \end{pmatrix} \quad \phi_2 = \begin{pmatrix} e^{Ah} & -\Lambda \\ 0 & -I \end{pmatrix} \tag{19}$$

where $\Lambda := \int_0^h e^{As}dsBK$. Thus, for an augmented state $w(kh) = [x(kh), \hat{x}(kh)]^{\rm T}$, let the closed-loop system be defined by

$$w\left((k+1)h\right) = \phi_j w(kh) \tag{20}$$

where $j = 1, 2$ and $\tilde{x}(kh) = x(kh)$ for $j = 1$ and $\tilde{x}(kh) = x((k-1)h)$ for $j = 2$. Thus, $j = 1$ represents the system when

the packet is transmitted successfully, and $j = 2$ represents the system when the packet has been dropped. Assume that the plant states are transmitted at a rate r; then, if there exists a Lyapunov function $V(w(kh)) = w^{\mathrm{T}}(kh)Pw(kh)$ and scalars α_1 and α_2 for (20) such that

$$\alpha_1^r \alpha_2^{r-1} > 1 \quad \phi_1^{\mathrm{T}} P \phi_1 \leq \alpha_1^{-2} P \quad \phi_2^{\mathrm{T}} P \phi_2 \leq \alpha_2^{-2} P \tag{21}$$

the system is exponentially stable (see [21]). Using Lyapunov functions, [22] and [23] analyzed a system where packet dropouts occur in both the sensor-to-controller and controller-to-actuator links.

3) Delays: Latency in the communication channels can be either random or constant and either bounded or unbounded. These depend on the medium access control protocol. Common multiple access protocols for wired or wireless networks include carrier sense multiple access (CSMA), time division multiple access (TDMA), token bus, token ring, and token passing. NCS using CSMA protocols such as controller area network or Ethernet involves uncertain or random delays for a large number of nodes and arrival rates [27]. TDMA or token-type protocols, commonly used in fiber optic networks, involve a more deterministic type of latency.

In [24], the stability of an NCS based on a bounded delay $\tau \in [a\ b]$ for $a, b \in \mathbb{R}^+$, was studied based on the linear matrix inequalities, the Lyapunov functions, and the Jordan canonical form of the system in (16).

This paper focuses on studying the impact of fixed communication delay in the controller shown in Fig. 9 to the entire system. In [6], a straightforward approach to model this delay was illustrated based on the assumption that the total delay $\tau := \tau_{sc} + \tau_{ca}$ is bounded and is of the following form $\tau = lT_s - mT_s$, where $l \in \mathbb{N}$, $m \in (0, 1)$, and fixed network sampling time $T_s \in \mathbb{R}_{>0}$. The entire system is modeled as in (15), with the exception that, in the LES controller shown in Fig. 3(a), i'_L is left for feedback as $\tilde{d} = i'_L k_p - \tilde{i}_L k_p$.

Therefore, (15) is modified to include the inner control loop shown in Fig. 9, and the new input to the LES boost converter becomes i'_L. The new linearized model for the charging facility is then written as

$$\dot{\tilde{x}} = A\tilde{x} + b_i i'_L + B\mu \tag{22}$$

where $\mu = [\tilde{V}_{\mathrm{dc}}^L, \tilde{V}_{\mathrm{dc}}^P, \hat{I}_{dq}]^{\mathrm{T}}$ and B are the same disturbances and matrix as in (15). For simplicity, we assume that there are no external disturbances, i.e., $\mu \equiv 0$. The solution to (22) is of the following form:

$$\tilde{x}(t) = e^{A(t-t_0)}\tilde{x}(t_0) + \int_{t_0}^{t} e^{A(t-\eta)} b_i i'_L(\eta) d\eta. \tag{23}$$

Let $t_0 := kT_s$, $t := (k+1)T_s$, and $\eta := \beta + kT_s$ to discretize the solution

$$x\left((k+1)T_s\right) = e^{AT_s} x(kT_s) + \int_0^{T_s} e^{A(T_s-\beta)} b_i i'_L(\beta + kT_s) d\beta. \tag{24}$$

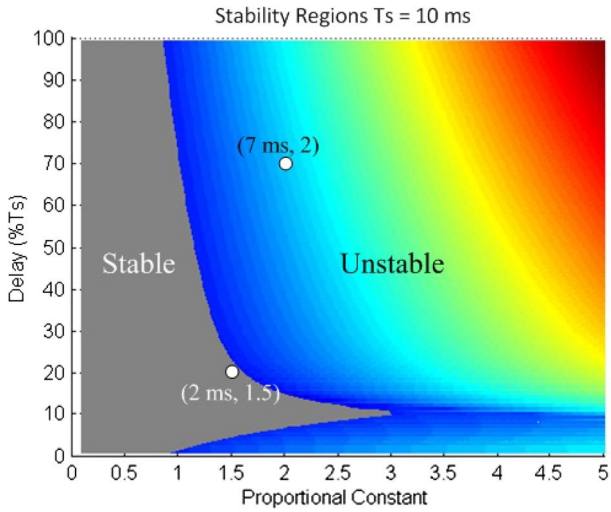

Fig. 10. Local stability regions based on a network sampling time and outer proportional constant K of controller in Fig. 9.

Assuming that $l = 1$, then the delay is bounded within one time step $\tau = (1-m)T_s$, and as such, we can separate the integral in (24) into two parts: one for the previous input $i'_L((k-1)T_s)$ and the other one for the current input $i'_L(kT_s)$

$$x\left((k+1)T_s\right) = e^{AT_s} x(kT_s) + \Phi_1 i'_L\left((k-1)T_s\right) + \Phi_2 i'_L(kT_s) \tag{25}$$

where $\Phi_1 := \int_0^{pT_s} e^{A(T_s-\beta)} d\beta\ b_i$, $\Phi_2 := \int_{pT_s}^{T_s} e^{A(T_s-\beta)} d\beta b_i$, and $p := (1-m)$. Using a controller of the form $i'_L(k) = -K_N x(k)$, we can obtain the closed-loop system

$$\begin{pmatrix} x(k+1) \\ i'_L(k) \end{pmatrix} = \begin{pmatrix} e^{AT_s} - \Phi_2 K_N & \Phi_1 \\ -K_N & 0 \end{pmatrix} \begin{pmatrix} x(k) \\ i'_L(k-1) \end{pmatrix}. \tag{26}$$

C. Stability Analysis

In this section, the stability of the charging facility with respect to network sampling time and delay is studied. In general, we can deduce that the linearized model of the charging facility is locally exponentially stable about the operating point x^* if the state matrix denoted by A_{cl} in (26) is Hurwitz, i.e., $|\lambda| < 1$, $\forall \lambda \in \sigma(A_{cl})$. Using a network sampling time of $T_s = 10$ ms, the stability regions for which the PHEV charging facility is *locally exponentially stable* based on the networked control parameter and delay are shown in Fig. 10.

The intensity of the colors in Fig. 10 is related to the absolute value of the largest eigenvalue $|\lambda| > 1$. It can be seen that, for certain delays and control parameters, the system may eventually go unstable. For systems with network sensing and control, it is particularly important to have bounds on the delay and control parameters in order to establish a stable operation.

IV. Real-Time Simulation Platform

The PHEV charging station considered consists of two DERs, LES and PV, as well as multiple power converters, critical loads, PHEV charging stations, and batteries. Thus, a large-scale microgrid test bed is not economically feasible. For

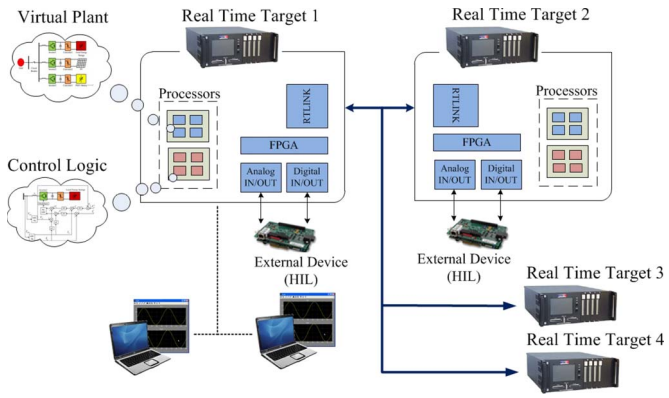

Fig. 11. Real-time simulation platform for electrical network modeling.

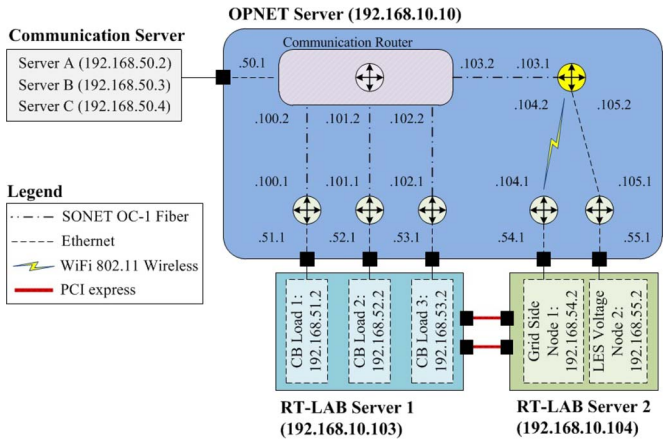

Fig. 12. Combination of electrical and communication network systems.

example, there are only a handful test platforms around the world [25], [26]. For this reason, in order to validate the stability analysis of the NCS case inasmuch realistic setting as possible, a real-time simulation platform that combines both electrical and communication network models has been developed [27].

A. Electrical Network Simulation

The real-time simulation platform of the electrical system is CPU based running a Linux operating system from Opal RT [28]. In total, there are four real-time simulators with a total of 8 CPUs, 48 cores, 5 FPGA chips, and more than 500 analog and digital inputs/outputs. Dolphin [29] PCI boards are used to provide an extremely high-speed and low-latency real-time communication link between the simulators.

The main challenge in simulating models with high-speed switching devices is the small step size required to achieve adequate simulation accuracy. For example, assuming that the switching time step of a power converter is $T_{sw} = 100\ \mu$s, the simulation time step T_s should be at least $T_s \leq T_{sw}/10 = 10\ \mu$s in order to produce accurate results of the switching transients and the larger system.

Currently, there are two solutions to this problem. The first solution uses switch event interpolation technology which combines software solving algorithms with high-end hardware. The RT-EVENTS software library [28] in combination with FPGA is used to handle discrete events that occur inside one model calculation step. In this case, the switching events are logged by the FPGA which runs at a much faster clock cycle, e.g., $T_s = 10$ ns for a Xilinx Spartan 3 chip, and the average is sent to the CPU model at the beginning of each model step. The second solution involves directly modeling the entire system inside an FPGA chip. Both solutions produce accurate results of the power network being modeled.

Furthermore, relying on the parallel computation capability, this platform is able to run a complex power system model with a maximum of 48 subsystems, which can further increase the switching frequency and number of switching devices in the model. Each subsystem can represent either a DER, a controller unit, and/or PHEV loads. The electrical network simulation platform is summarized in Fig. 11.

In general, with the help of the presented real-time simulation system, a switching frequency of up to 10 kHz can be achieved,

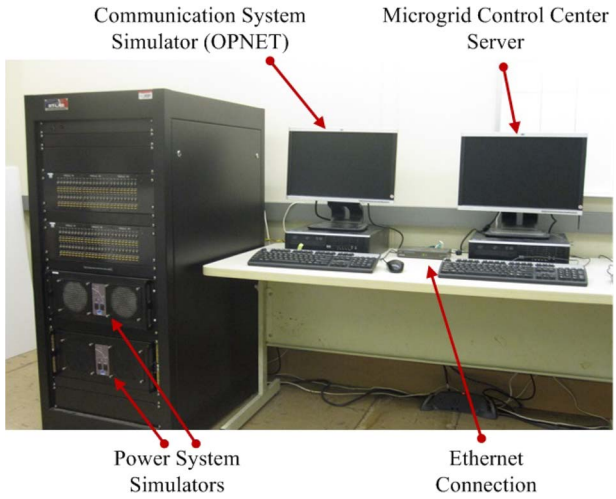

Fig. 13. Real-time simulation platform of the PHEV charging facility and communication network.

TABLE II
REAL-TIME SIMULATION PARAMETERS

Network Parameters			
Sampling time T_{sn}	10 ms	Total delay τ	$2-9$ ms
Remote k_p	$0.5-5$		
Electrical Parameters			
PV $V_{dc_{\text{MPPT}}}$	437 V	PV $i_{L_{\text{MPPT}}}$	7.6 A
LES, PV v_C	800 V	Ac Bus V_{gd}	240 V_{rms}
LES V_{dc}	212 V	Critical Load r_N	1000 Ω
Load Dist. $\hat{I}_d$	16.67 A	Fund. Frequency	60 Hz
Filter R_f	1 mΩ	Filter L_f	0.76 mH
Filter C_f	3.451 μF	Line R_c	1 mΩ
Line L_c	0.76 mH	Simulation T_s	50 μs

and a large number of switches can be included in one model. Moreover, the system allows multiple users to be connected to the real-time simulator concurrently to perform collaborative simulation, for which distributed control and hardware-in-the-loop (HIL) operation can be easily realized.

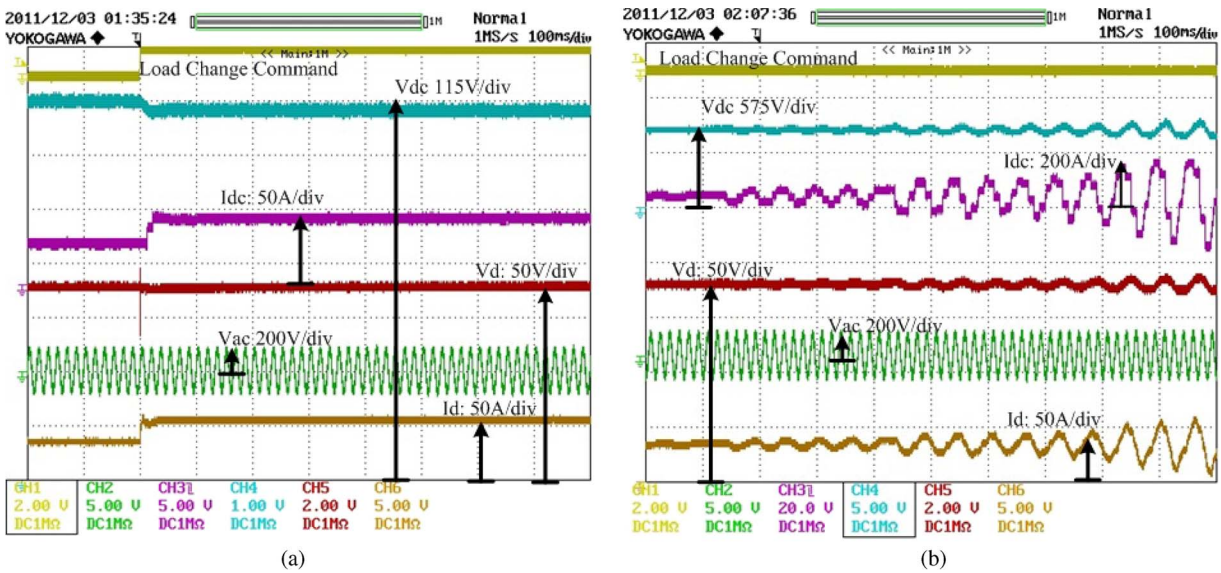

Fig. 14. Real-time simulation results for stable and unstable NCSs during load change. (a) $T_s = 10$ ms, $\tau = 2$ ms, and $kp_v = 1.5$. (b) $T_s = 10$ ms, $\tau = 7$ ms, and $kp_v = 2$.

B. Communication Network Simulation

Current network emulators offer the capability to be integrated with real hardware and devices under test. In academia, one of the most prevalent tools is NS2 [31]. NS2 is an open-source network simulation package which has the capability to operate as a system-in-the-loop (SITL) emulator. It is able to accept real-time network traffic and to simulate either wired or wireless networks. In addition, the live traffic can either be interpreted as opaque data packet (opaque mode) or protocol data packets which can be manipulated by the software (protocol mode). Another type of network emulator is Exata [32], developed by Scalable Network Technologies based on the popular QualNet. Exata is able to simulate parameters such as terrain, cyber attacks, scalability, and static parameters. While Exata can be used in SITL applications, it is mainly directed toward the military industry. Furthermore, Exata's university licensing offers mainly precompiled code with little adaptability and flexibility compared to the open-source solutions presented.

OPNET [33] is a well-developed commercially available network simulator that has been used extensively in research. There is a large community of support available for OPNET modeler comparable to NS2. However, being a commercial product, corporate support through OPNET Technologies is available as well. An SITL package is available for use with OPNET that bridges its network simulation with the electrical network simulation platform described in the previous section. The university license for OPNET allows significant flexibility in terms of network development; this, combined with the integrated support of many well-known communication protocols, makes OPNET an excellent option for implementation of the communication network.

V. Stability Analysis Validation

The PHEV charging facility model shown in Fig. 8 is built using the proposed real-time simulator. The model including the communication network is shown in Fig. 12. The system is split into two different targets in order to help decrease the simulation time step while avoiding overruns. RT-Lab server 2 is used to model the LES and PV DERs, whereas the PHEV charging stations and their respective power converters are modeled in server 1. Although only two nodes are needed for the NCS case presented in Fig. 9, i.e., the sensor-actuator and the control center, different nodes in Fig. 12 represent the circuit breakers which enhances the control center capabilities to connect and disconnect loads and DERs.

In the simulation environment, multiple gateways can be connected to a single physical Ethernet port. Each gateway is assigned a filter to only allow network traffic from a specific IP address, TCP, or UDP port or even for a specific application to enter OPNET simulation. In Fig. 12, six gateways are defined to accept traffic from six external nodes. Each node is configured to be on a separate IP subnet. Furthermore, in this example, there are three different kinds of networks being emulated: fiber optic, wireless, and wired. Finally, by placing each network node at different distances from each other, the delays which would occur in an actual system can be simulated depending on the types of link used. Factors such as bandwidth, jitter, and packet losses are controllable as well. The actual platform is shown in Fig. 13. The charging facility and control parameters are shown in Table II.

The real-time simulation results are presented in Fig. 14. Fig. 14(a) corresponds to the point in Fig. 10 located in the stable region, i.e., for $T_s = 10$ ms, $\tau = 2$ ms, and $kp_v = 1.5$. The yellow trace represents a load change disturbance added to the system to verify the local stability properties. The red and green traces represent the ac bus voltage in dq and ac format, respectively.

In Fig. 14(b), the unstable region of the system was simulated. In this case, $T_s = 10$ ms, $\tau = 7$ ms, and $kp_v = 2$, where it can be seen clearly that the RT simulation is also unstable.

VI. Conclusion

In this paper, the small-signal analysis and the proposed NCS of a PHEV charging facility have been presented. The linearized model of the charging facility, including both dc/dc and dc/ac converters, has been derived, and the stability of the system without communication has been studied.

For the case with networked control, a review of the challenges and opportunities in NCS has been presented. In addition, the LES dc bus voltage with the outer control loop going to a control center with a communication link has been proposed. The stability of the charging facility based on this NCS is studied for a fixed delay. This type of delay can be achieved using fiber optic links and token ring or token bus protocols. Based on a network sampling time of $T_s = 10$ ms, boundaries of operation based on delay and control parameters were obtained.

A real-time simulation platform has been presented, which is able to model both electrical and communication network dynamics. This platform is then used to validate the stability regions based on the networked control of the dc bus voltage.

In the future, more in-depth analysis of control schemes for charging facilities involving multiple-input–multiple-output NCS will be analyzed following a similar approach as the one presented in this paper. Transmission times, packet losses, and delays will be taken into account using the reviewed methods.

References

[1] J. Tomic and W. Kempton, "Using fleets of electric-drive vehicles for grid support," *J. Power Sources*, vol. 168, no. 2, pp. 459–468, Jun. 2007.

[2] T. Markel, M. Kuss, and P. Denholm, "Communication and control of electric drive vehicles supporting renewables," in *Proc. IEEE Veh. Power Propulsion Conf.*, 2009, pp. 27–34.

[3] P. Kulshrestha, K. Swaminathan, M. Chow, and S. Lukic, "Evaluation of ZigBee communication platform for controlling the charging of PHEVs at a municipal parking deck," in *Proc. IEEE Veh. Power Propulsion Conf.*, 2009, pp. 1211–1214.

[4] F. Katiraei, M. Iravani, and P. Lehn, "Small-signal dynamic model of a micro-grid including conventional and electronically interfaced distributed resources," *IET Gener. Transm. Distrib.*, vol. 1, no. 3, pp. 369–378, May 2007.

[5] N. Pogaku, M. Prodanovic, and T. Green, "Modeling, analysis and testing of autonomous operation of an inverter-based microgrid," *IEEE Trans. Power Electron.*, vol. 22, no. 2, pp. 613–625, Mar. 2007.

[6] M. Branicky, S. Phillips, and W. Zhang, "Stability of networked control systems: Explicit analysis of delay," in *Proc. Amer. Control Conf.*, 2000, pp. 2352–2357.

[7] S. Mazumder, M. Tahir, and S. Kamisetty, "Wireless PWM control of a parallel dc–dc buck converter," *IEEE Trans. Power Electron.*, vol. 20, no. 6, pp. 1280–1286, Nov. 2005.

[8] S. Wang, X. Meng, and T. Chen, "Wide-area control of power systems through delayed network communications," *IEEE Trans. Control Syst. Technol.*, vol. 20, no. 2, pp. 495–503, Mar. 2012.

[9] Q. Shafiee, J. Vasquez, and J. Guerrero, "Distributed secondary control for islanded microgrids—A networked control systems approach," in *Proc. 38th Annu. IEEE IECON*, 2012, pp. 5637–5642.

[10] G. Preetham and W. Shireen, "Photovoltaic charging station for plug-in hybrid electric vehicles in a smart grid environment," in *Proc. IEEE PES Innovative Smart Grid Technol.*, 2012, pp. 1–8.

[11] S. Bai, Y. Du, and S. Lukic, "Optimum design of an EV/PHEV charging station with dc bus and storage system," in *Proc. IEEE ECCE*, 2010, pp. 1178–1184.

[12] F. Huang, P. Sarikprueck, Y. Cheng, and W. Lee, "Design optimization of PHEV charging station," in *Proc. IEEE I&CPS*, 2012, pp. 1–7.

[13] K. Morrow, D. Karner, and J. Francfort, "Plug-in hybrid electric vehicle charging infrastructure review," U.S. Dept. Energy, Assistant Secretary Energy Efficiency Renew. Energy, DOE Idaho Oper. Off., Washington, DC, USA, Rep. INL/EXT-08-15 058, 2008.

[14] R. D. Middlebrook and S. Cuk, "A general unified approach to modelling switching-converter power stages," in *Proc. IEEE Power Electron. Spec. Conf.*, 1976, pp. 18–34.

[15] C. Rim, D. Hu, and G. Cho, "Transformers as equivalent circuits for switches: General proofs and $d-q$ analyses," *IEEE Trans. Ind. Appl.*, vol. 26, no. 4, pp. 777–785, Jul./Aug. 1990.

[16] J. Undrill, "Dynamic stability calculations for an arbitrary number of interconnected synchronous machines," *IEEE Trans. Power App. Syst.*, vol. PAS-87, no. 3, pp. 835–844, Mar. 1968.

[17] G. Walsh, H. Ye, and L. Bushnell, "Stability analysis of networked control systems," *IEEE Trans. Control Syst. Technol.*, vol. 10, no. 3, pp. 438–446, May 2002.

[18] W. Zhang, "Stability analysis of networked control systems," Ph.D. dissertation, Dept. Elect. Comput. Sci., Case Western Reserve Univ., Cleveland, OH, USA, 2001.

[19] D. Nesic and A. Teel, "Input–output stability properties of networked control systems," *IEEE Trans. Autom. Control*, vol. 49, no. 10, pp. 1650–1667, Oct. 2004.

[20] W. Heemels, A. Teel, N. van de Wouw, and D. Nesic, "Networked control systems with communication constraints: Tradeoffs between transmission intervals, delays and performance," *IEEE Trans. Autom. Control*, vol. 55, no. 8, pp. 1781–1796, Aug. 2010.

[21] A. Hassibi, S. Boyd, and J. How, "Control of asynchronous dynamical systems with rate constraints on events," in *Proc. IEEE Conf. Decision Control*, 1999, pp. 1345–1351.

[22] W. Zhang and L. Yu, "Output feedback stabilization of networked control systems with packet dropouts," *IEEE Trans. Autom. Control*, vol. 52, no. 9, pp. 1705–1710, Sep. 2007.

[23] J. Wu and T. Chen, "Design of networked control systems with packet dropouts," *IEEE Trans. Autom. Control*, vol. 52, no. 7, pp. 1314–1319, Jul. 2007.

[24] M. Cloosterman, N. van de Wouw, W. Heemels, and H. Nijmeijer, "Stability of networked control systems with uncertain time-varying delays," *IEEE Trans. Autom. Control*, vol. 54, no. 7, pp. 1575–1580, Jul. 2009.

[25] R. H. Lasseter, J. H. Eto, B. Schenkman, J. Stevens, H. Vollkommer, D. Klapp, E. Linton, H. Hurtado, and J. Roy, "CERTS microgrid laboratory test bed," *IEEE Trans. Power Del.*, vol. 26, no. 1, pp. 325–332, Jan. 2011.

[26] M. Mao, M. Ding, J. Su, L. Chang, M. Sun, and G. Zhang, "Testbed for microgrid with multi-energy generators," in *Proc. IEEE Can. Conf. Elect. Comput. Eng.*, 2008, pp. 637–640.

[27] F. Guo, L. Herrera, R. Murawski, E. Inoa, P. Beauchamp, E. Ekici, and J. Wang, "Comprehensive real time simulations of smart grid," *IEEE Trans. Ind. Appl.*, vol. 49, no. 2, pp. 899–908, Mar./Apr. 2013.

[28] Opal-RT Technologies. [Online]. Available: http://www.opalrt.com

[29] Dolphin. [Online]. Available: http://www.dolphinics.com

[30] P. Parikh, M. Kanabar, and T. Sidhu, "Opportunities and challenges of wireless communication technologies for smart grid applications," in *Proc. CCECS Energy Soc. Gen. Meet.*, 2010, pp. 1–7.

[31] Network Emulation With the NS Simulator. [Online]. Available: http://www.isi.edu/nsnam/ns/ns-emulation.html

[32] Exata 2011. [Online]. Available: http://www.scalable-networks.com

[33] OPNET 2011. [Online]. Available: http://www.opnet.com

Luis Herrera (S'10) received the B.S. degree in electrical engineering with a minor in physics from the University of Tennessee at Martin, Martin, TN, USA, in 2010. Since 2010, he has been working toward the Ph.D. degree at The Ohio State University, Columbus, OH, USA.

His current research interests include modeling and networked control of the smart grid, FPGA modeling of fast switching power converters, hardware-in-the-loop simulations, and active power filtering.

Ernesto Inoa (S'10–M'12) was born in the Dominican Republic. He received the B.S. degree in electronics engineering (*magna cum laude*) from the Pontificia Universidad Católica Madre y Maestra, Santiago de Los Caballeros, Dominican Republic, in 2000, the M.S. degree in electrical and computer engineering from the University of Central Florida, Orlando, FL, USA, in 2005, and the Ph.D. degree from The Ohio State University, Columbus, OH, USA, in 2012.

From 2000 to 2002, he was an Automation Engineer with CND, a Dominican brewing company, where he helped to automate several bottling lines with the use of programmable logic controllers. Since July 2012, he has been an R&D Engineer with Caterpillar, Inc., Peoria, IL, USA, where he is researching control algorithms for the power electronics systems of the next generation of hybrid electric trucks and tractors. His major research interests are related to the application of advanced control theory and digital signal processing techniques to power electronics, motor drives, and energy conversion systems.

Dr. Inoa received the Best Student Presentation Award at ECCE 2011, Phoenix, AZ, USA.

Feng Guo (S'09) was born in Henan, China, in 1986. He received the B.S. degree in electrical engineering from Wuhan University, Wuhan, China, in 2009. He is currently working toward the Ph.D. degree at The Ohio State University, Columbus, OH, USA.

His current research interests include large-scale PV power plants, hardware-in-the-loop and real-time simulation of smart grid, power electronics circuits in hybrid electric vehicles, and energy harvesting around high-voltage transmission lines.

Jin Wang (S'02–M'05) received the B.S. degree in electrical engineering from Xi'an Jiaotong University, Xi'an, China, in 1998, the M.S. degree in electrical engineering from Wuhan University, Wuhan, China, in 2001, and the Ph.D. degree in electrical engineering from Michigan State University, East Lansing, MI, USA, in 2005.

From September 2005 to August 2007, he was a Core Power Electronics Engineer with Ford Motor Company, Dearborn, MI, USA, where he contributed to the traction drive design of the Ford Fusion Hybrid. In September 2007, he became an Assistant Professor with the Department of Electrical and Computer Engineering, The Ohio State University, Columbus, OH, USA. He was promoted to Associate Professor with tenure in 2013.

Dr. Wang received the IEEE Power Electronics Society Richard M. Bass Young Engineer Award and the National Science Foundation's CAREER Award in 2011, Ralph L. Boyer Award for Excellence in Undergraduate Teaching Innovation in 2012, and the Lumley Research Award of the College of Engineering, The Ohio State University, in 2013. He has been an Associate Editor of the IEEE TRANSACTIONS ON INDUSTRY APPLICATIONS since March 2008.

Hanning Tang (S'10–M'12) received the B.S. degree from Southeast University, Nanjing, China, in 2010 and the M.S. degree from The Ohio State University, Columbus, OH, USA, in 2012.

Since 2012, he has been with Eaton Corporation, Arden, NC, USA, where he is currently a Senior Design Engineer with the Power Distribution and Control Assemblies Division. His design and research interests include energy conversion, electric machines, and power electronics with applied modern control theories.